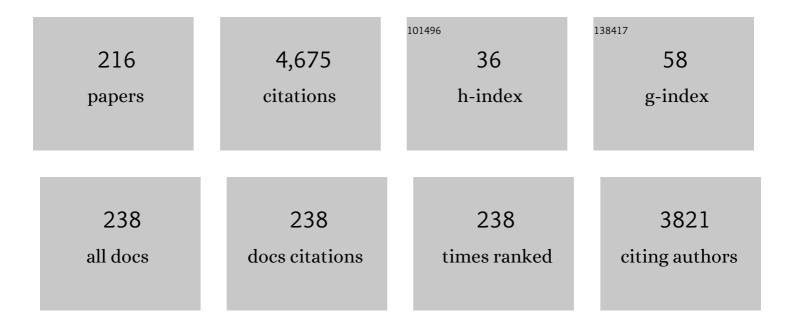
Takeshi Tsuji

List of Publications by Year in descending order

Source: https://exaly.com/author-pdf/7636808/publications.pdf Version: 2024-02-01



Τλάξομι Τοιιίι

#	Article	IF	CITATIONS
1	Influence of pore space heterogeneity on mineral dissolution and permeability evolution investigated using lattice Boltzmann method. Chemical Engineering Science, 2022, 247, 117048.	1.9	15
2	Elastic Wave Velocity Changes Due to the Fracture Aperture and Density, and Direct Correlation With Permeability: An Energetic Approach to Mated Rock Fractures. Journal of Geophysical Research: Solid Earth, 2022, 127, .	1.4	9
3	Achieving a Carbon Neutral Future through Advanced Functional Materials and Technologies. Bulletin of the Chemical Society of Japan, 2022, 95, 73-103.	2.0	39
4	A coupled LBM-DEM method for simulating the multiphase fluid-solid interaction problem. Journal of Computational Physics, 2022, 454, 110963.	1.9	27
5	Pore fabric anisotropy and elastic moduli of fault rocks from the Median Tectonic Line, Shikoku, southwest Japan. Tectonophysics, 2022, 834, 229366.	0.9	0
6	Accurate determination of the first arrival time of elastic wave traveled through rock sample by machine learning. Journal of Applied Geophysics, 2022, 203, 104688.	0.9	3
7	Relative Permeability Variation Depending on Viscosity Ratio and Capillary Number. Water Resources Research, 2022, 58, .	1.7	6
8	Mapping the geological structures in the Ras El Ush field (Gulf of Suez, Egypt), based on seismic interpretation and 3D modeling techniques. Journal of African Earth Sciences, 2022, 193, 104596.	0.9	8
9	Spatial and temporal influence of sea level on inland stress based on seismic velocity monitoring. Earth, Planets and Space, 2022, 74, .	0.9	0
10	Ambient noise tomography for a high-resolution 3D S-wave velocity model of the Kinki Region, Southwestern Japan, using dense seismic array data. Earth, Planets and Space, 2022, 74, .	0.9	7
11	Spatiotemporal Variations of Soil Moisture and Groundwater Level in a South Sumatra Peatland, Indonesia During 2015–2018. Geography, Environment, Sustainability, 2022, 15, 58-70.	0.6	1
12	Investigation of viscous coupling effects in three-phase flow by lattice Boltzmann direct simulation and machine learning technique. Advances in Water Resources, 2021, 147, 103797.	1.7	13
13	Relating Hydraulic–Electrical–Elastic Properties of Natural Rock Fractures at Elevated Stress and Associated Transient Changes of Fracture Flow. Rock Mechanics and Rock Engineering, 2021, 54, 2145-2164.	2.6	17
14	Influence of structure and pore pressure of plate interface on tectonic tremor in the Nankai subduction zone, Japan. Earth and Planetary Science Letters, 2021, 558, 116742.	1.8	5
15	Spatial autocorrelation method for reliable measurements of two-station dispersion curves in heterogeneous ambient noise wavefields. Geophysical Journal International, 2021, 226, 1130-1147.	1.0	3
16	Traffic Monitoring System Based on Deep Learning and Seismometer Data. Applied Sciences (Switzerland), 2021, 11, 4590.	1.3	15
17	High Fluidâ€Pressure Patches Beneath the Décollement: A Potential Source of Slow Earthquakes in the Nankai Trough off Cape Muroto. Journal of Geophysical Research: Solid Earth, 2021, 126, e2021JB021831.	1.4	11
18	Geological storage of CO ₂ –N ₂ –O ₂ mixtures produced by membraneâ€based direct air capture (DAC). , 2021, 11, 610-618.		17

#	Article	IF	CITATIONS
19	Scale-independent relationship between permeability and resistivity in mated fractures with natural rough surfaces. Geothermics, 2021, 94, 102065.	1.5	21
20	Flow estimation solely from image data through persistent homology analysis. Scientific Reports, 2021, 11, 17948.	1.6	16
21	Continuous monitoring system for safe managements of CO2 storage and geothermal reservoirs. Scientific Reports, 2021, 11, 19120.	1.6	13
22	Pore pressure and gas saturation distribution in the forearc basin of the Nankai subduction zone inferred from high-resolution Vp and Vs. Journal of Petroleum Science and Engineering, 2021, 205, 108911.	2.1	10
23	Machine learning for automatic slump identification from 3D seismic data at convergent plate margins. Marine and Petroleum Geology, 2021, 133, 105290.	1.5	4
24	Elucidation of pore connection mechanism during ductile fracture of sintered pure iron by applying persistent homology to 4D images of pores: Role of open pore. Materials Science & Engineering A: Structural Materials: Properties, Microstructure and Processing, 2021, 828, 142112.	2.6	5
25	Mapping Aquifer Storage Properties Using S-Wave Velocity and InSAR-Derived Surface Displacement in the Kumamoto Area, Southwest Japan. Remote Sensing, 2021, 13, 4391.	1.8	4
26	Temporal changes in anthropogenic seismic noise levels associated with economic and leisure activities during the COVID-19 pandemic. Scientific Reports, 2021, 11, 20439.	1.6	6
27	Mapping aquifer storage properties using S-wave velocity and InSAR measurements in the Kumamoto area, Japan. , 2021, , .		0
28	Three-dimensional S-wave velocity structure of the Kinki Region, southwestern Japan with ambient seismic noise tomography using a dense seismic array. , 2021, , .		0
29	Characterization and utilization of heterogeneous ambient noise field for imaging subsurface structure in the Itoshima Peninsula, Japan. , 2021, , .		0
30	Digital rock physics revealing the relationships between permeability, resistivity and elastic wave velocity of rock fractures. , 2021, , .		0
31	Miniature seismometer array system for Lunar underground structures investigation: Evaluation of its exploration depth based on Apollo seismometer data. BUTSURI-TANSA(Geophysical Exploration), 2021, 74, 79-91.	0.0	0
32	Vehicles detection based on their seismic surface waves using classification techniques. , 2021, , .		1
33	Peatland subsidence and vegetation cover degradation as impacts of the 2015 El niño event revealed by Sentinel-1A SAR data. International Journal of Applied Earth Observation and Geoinformation, 2020, 84, 101953.	1.4	11
34	Two-station continuous wavelet transform cross-coherence analysis for surface-wave tomography using active-source seismic data. Geophysics, 2020, 85, EN17-EN28.	1.4	8
35	Microsecond simulation study on the replacement of methane in methane hydrate by carbon dioxide, nitrogen, and carbon dioxide–nitrogen mixtures. Fuel, 2020, 263, 116640.	3.4	35
36	Extracting surface wave dispersion curves from two-station microtremor analysis in heterogeneous ambient noise wavefield. , 2020, , .		0

#	Article	IF	CITATIONS
37	Data processing and interpretation schemes for a deep-towed high-frequency seismic system for gas and hydrate exploration. Journal of Natural Gas Science and Engineering, 2020, 83, 103573.	2.1	5
38	Pore Pressure Analysis for Distinguishing Earthquakes Induced by CO2 Injection from Natural Earthquakes. Sustainability, 2020, 12, 9723.	1.6	4
39	Inferring fracture forming processes by characterizing fracture network patterns with persistent homology. Computers and Geosciences, 2020, 143, 104550.	2.0	12
40	Impacts of COVID-19 on a Transitioning Energy System, Society, and International Cooperation. Sustainability, 2020, 12, 8232.	1.6	25
41	Permanent monitoring system using continuous and controlled seismic source: Monitoring of dynamic behaviors from smaller reservoir to larger crust. , 2020, , .		0
42	Overpressured Underthrust Sediment in the Nankai Trough Forearc Inferred From Transdimensional Inversion of Highâ€Frequency Teleseismic Waveforms. Geophysical Research Letters, 2020, 47, e2020GL088280.	1.5	21
43	Characterizing coal seams hosted in Mmamabula Coalfield, central Botswana using pseudo-3D electrical resistivity imaging technique. Journal of African Earth Sciences, 2020, 167, 103866.	0.9	5
44	Temporal Variation and Frequency Dependence of Seismic Ambient Noise on Mars From Polarization Analysis. Geophysical Research Letters, 2020, 47, e2020GL087123.	1.5	24
45	Sound speed of thermohaline fine structure in the Kuroshio Current inferred from automatic sound speed analysis. Exploration Geophysics, 2020, 51, 581-590.	0.5	3
46	Distributions of gas hydrate and free gas accumulations associated with upward fluid flow in the Sanriku-Oki forearc basin, northeast Japan. Marine and Petroleum Geology, 2020, 116, 104305.	1.5	16
47	Threeâ€Ðimensional <i>S</i> Wave Velocity Structure of Central Japan Estimated by Surfaceâ€Wave Tomography Using Ambient Noise. Journal of Geophysical Research: Solid Earth, 2020, 125, e2019JB019043.	1.4	16
48	Seasonal and transient surface displacements in the Kumamoto area, Japan, associated with the 2016 Kumamoto earthquake: implications for seismic-induced groundwater level change. Earth, Planets and Space, 2020, 72, .	0.9	6
49	Spatial and temporal influence of rainfall on crustal pore pressure based on seismic velocity monitoring. Earth, Planets and Space, 2020, 72, .	0.9	22
50	Identification of a nascent tectonic boundary in the San-in area, southwest Japan, using a 3D S-wave velocity structure obtained by ambient noise surface wave tomography. Earth, Planets and Space, 2020, 72, .	0.9	12
51	Real-time crustal monitoring system of Japanese Islands based on spatio-temporal seismic velocity variation. Earth, Planets and Space, 2020, 72, .	0.9	8
52	Continuous reservoir monitoring system based on permanent seismic source and distributed acoustic sensing. , 2020, , .		2
53	Multichannel analysis of surface waves with continuous wavelet transform for near surface applications. , 2020, , .		0
54	Migration of Very Long Period Seismicity at Aso Volcano, Japan, Associated With the 2016 Kumamoto Earthquake. Geophysical Research Letters, 2019, 46, 8763-8771.	1.5	11

#	Article	IF	CITATIONS
55	Internal Structure of a Seafloor Massive Sulfide Deposit by Electrical Resistivity Tomography, Okinawa Trough. Geophysical Research Letters, 2019, 46, 11025-11034.	1.5	28
56	Underground structures associated with horizontal sliding at Uchinomaki hot springs, Kyushu, Japan, during the 2016 Kumamoto earthquake. Earth, Planets and Space, 2019, 71, .	0.9	3
57	Large Gas Reservoir Along the Rift Axis of a Continental Backâ€Arc Basin Revealed by Automated Seismic Velocity Analysis in the Okinawa Trough. Geophysical Research Letters, 2019, 46, 9583-9590.	1.5	9
58	Grid-search inversion based on rock physics model for estimation of pore geometry and grain elastic moduli: application to hydrothermal ore deposits and basalt. Exploration Geophysics, 2019, 50, 1-11.	0.5	4
59	Ab Initio Molecular Dynamics Study of Carbonation and Hydrolysis Reactions on Cleaved Quartz (001) Surface. Journal of Physical Chemistry C, 2019, 123, 4938-4948.	1.5	12
60	Surface wave analysis for heterogeneous geological formations in geothermal fields: effect of wave propagation direction. Exploration Geophysics, 2019, 50, 255-268.	0.5	7
61	Four-dimensional observation of ductile fracture in sintered iron using synchrotron X-ray laminography. Powder Metallurgy, 2019, 62, 146-154.	0.9	4
62	Evolution of hydraulic and elastic properties of reservoir rocks due to mineral precipitation in CO2 geological storage. Computers and Geosciences, 2019, 126, 84-95.	2.0	20
63	Methane Concentration in Mud Conduits of Submarine Mud Volcanoes: A Coupled Geochemical and Geophysical Approach. Geochemistry, Geophysics, Geosystems, 2019, 20, 792-813.	1.0	6
64	Surface-wave phase velocity tomography using active-source seismic data. , 2019, , .		0
65	Lunar Active Seismic Profiler (LASP): Investigation of shallow regolith layer for resource exploration and base camp construction. , 2019, , .		3
66	Surface wave analysis using active-source multi-channel seismic data in the Median Tectonic Line (MTL): Comparison of S-wave velocity along the MTL. , 2019, , .		0
67	Mapping Surface Displacements and Aquifer Characteristics Around the Kumamoto Plain, Japan, Using Persistent Scatterer Interferometry. , 2019, , .		2
68	Influence of faults and slumping on hydrocarbon migration inferred from 3D seismic attributes: Sanriku-Oki forearc basin, northeast Japan. Marine and Petroleum Geology, 2019, 99, 175-189.	1.5	14
69	Characterization of hydrate and gas reservoirs off Sanriku area from highresolution seismic velocity model. , 2019, , .		О
70	Evaluation of Optimal Processing Parameters for Automatic Continuous Monitoring Using Ambient Noise. , 2019, , .		1
71	Reflection mapping of oceanic thermohaline fine structure in the Kuroshio Current: Insights from automatic seismic velocity analysis. , 2019, , .		0
72	Digital rock approach for effective reservoir managements. Journal of the Japanese Association for Petroleum Technology, 2019, 84, 403-410.	0.0	0

#	Article	IF	CITATIONS
73	Characterization of hydrate and gas reservoirs in plate convergent margin by applying rock physics to high-resolution seismic velocity model. Marine and Petroleum Geology, 2018, 92, 719-732.	1.5	25
74	Temporal change in seismic velocity associated with an offshore MW 5.9 Off-Mie earthquake in the Nankai subduction zone from ambient noise cross-correlation. Progress in Earth and Planetary Science, 2018, 5, .	1.1	21
75	Punctuated growth of an accretionary prism and the onset of a seismogenic megathrust in the Nankai Trough. Progress in Earth and Planetary Science, 2018, 5, .	1.1	26
76	Imaging and monitoring of the shallow subsurface using spatially windowed surface-wave analysis with a single permanent seismic source. Geophysics, 2018, 83, EN23-EN38.	1.4	8
77	Surface-wave tomography for near-surface characterization with continuous-wavelet transform for two-station crosscorrelation. , 2018, , .		2
78	Characterization of Fluid Behavior in 3D Digitalized Fracture Using Lattice Boltzmann Method: Evolution of Permeability by Shear Deformation and Its Representative Elementary Volume. Journal of MMIJ, 2018, 134, 60-66.	0.4	1
79	Mathematical Modeling of Rock Pore Geometry and Mineralization: Applications of Persistent Homology and Random Walk. Mathematics for Industry, 2018, , 95-109.	0.4	3
80	Pore Geometry Characterization by Persistent Homology Theory. Water Resources Research, 2018, 54, 4150-4163.	1.7	26
81	Deep-biosphere methane production stimulated by geofluids in the Nankai accretionary complex. Science Advances, 2018, 4, eaao4631.	4.7	79
82	Study of the Nankai seismogenic fault using dynamic wave propagation modelling of digital rock from the Nobeoka Fault. Exploration Geophysics, 2018, 49, 11-20.	0.5	5
83	Gas hydrate saturation and distribution in the Kumano Forearc Basin of the Nankai Trough. Exploration Geophysics, 2017, 48, 137-150.	0.5	16
84	Elasticity and Stability of Clathrate Hydrate: Role of Guest Molecule Motions. Scientific Reports, 2017, 7, 1290.	1.6	41
85	Temporal variation of the shallow subsurface at the Aquistore CO ₂ storage site associated with environmental influences using a continuous and controlled seismic source. Journal of Geophysical Research: Solid Earth, 2017, 122, 2859-2872.	1.4	28
86	Influence of Slip Flow at Fluid-solid Interface upon Permeability of Natural Rock. Energy Procedia, 2017, 114, 3572-3577.	1.8	2
87	3D geometry of a plate boundary fault related to the 2016 Off-Mie earthquake in the Nankai subduction zone, Japan. Earth and Planetary Science Letters, 2017, 478, 234-244.	1.8	19
88	Hydraulic Properties of Closely Spaced Dipping Open Fractures Intersecting a Fluidâ€Filled Borehole Derived From Tube Wave Generation and Scattering. Journal of Geophysical Research: Solid Earth, 2017, 122, 8003-8020.	1.4	6
89	Robust Subsurface Monitoring Using a Continuous and Controlled Seismic Source. Energy Procedia, 2017, 114, 3956-3960.	1.8	2
90	Hydrologic and Elastic Properties of CO2 Injected Rock at Various Reservoir Conditions: Insights into Quantitative Monitoring of Injected CO2. Energy Procedia, 2017, 114, 4047-4055.	1.8	2

#	Article	IF	CITATIONS
91	Shallow characterization and monitoring of the Aquistore CO ₂ storage site from spatially windowed surface-wave analysis with a permanent seismic source. , 2017, , .		0
92	Horizontal sliding of kilometre-scale hot spring area during the 2016 Kumamoto earthquake. Scientific Reports, 2017, 7, 42947.	1.6	31
93	Spatial and temporal seismic velocity changes on Kyushu Island during the 2016 Kumamoto earthquake. Science Advances, 2017, 3, e1700813.	4.7	48
94	Impact of the kinetic boundary condition on porous media flow in the lattice Boltzmann formulation. Physical Review E, 2017, 96, 013303.	0.8	10
95	Ground uplift related to permeability enhancement following the 2011 Tohoku earthquake in the Kanto Plain, Japan. Earth, Planets and Space, 2017, 69, .	0.9	8
96	Modeling CO ₂ –Water–Mineral Wettability and Mineralization for Carbon Geosequestration. Accounts of Chemical Research, 2017, 50, 1530-1540.	7.6	80
97	Estimation of threeâ€phase relative permeability by simulating fluid dynamics directly on rockâ€microstructure images. Water Resources Research, 2017, 53, 11-32.	1.7	54
98	Time-lapse monitoring of shallow subsurface in the Aquistore CO ₂ storage site from surface-wave analysis using a continuous and controlled seismic source. , 2016, , .		4
99	Modeling and imaging of multiply generated and scattered tube waves due to multiple hydraulic fractures. , 2016, , .		0
100	Numerical investigations on the effect of initial state CO2 topology on capillary trapping efficiency. International Journal of Greenhouse Gas Control, 2016, 49, 179-191.	2.3	23
101	Distribution of stress state in the Nankai subduction zone, southwest Japan and a comparison with Japan Trench. Tectonophysics, 2016, 692, 120-130.	0.9	45
102	Characterization of immiscible fluid displacement processes with various capillary numbers and viscosity ratios in 3D natural sandstone. Advances in Water Resources, 2016, 95, 3-15.	1.7	145
103	Microscopic Origin of Strain Hardening in Methane Hydrate. Scientific Reports, 2016, 6, 23548.	1.6	15
104	Using seismic noise derived from fluid injection well for continuous reservoir monitoring. Interpretation, 2016, 4, SQ1-SQ11.	0.5	13
105	Surface wave attenuation in the shallow subsurface from multichannel–multishot seismic data: a new approach for detecting fractures and lithological discontinuities. Earth, Planets and Space, 2016, 68, .	0.9	12
106	Pixel-based interferometric pair selection in InSAR time-series analysis with baseline criteria. Remote Sensing Letters, 2016, 7, 711-720.	0.6	3
107	Development of surface-wave monitoring system for leaked CO2 using a continuous and controlled seismic source. International Journal of Greenhouse Gas Control, 2016, 45, 94-105.	2.3	8
108	Influence of fluid displacement patterns on seismic velocity during supercritical CO2 injection: Simulation study for evaluation of the relationship between seismic velocity and CO2 saturation. International Journal of Greenhouse Gas Control, 2016, 46, 197-204.	2.3	18

#	Article	IF	CITATIONS
109	Heterogeneous surface displacement pattern at the Hatchobaru geothermal field inferred from SAR interferometry time-series. International Journal of Applied Earth Observation and Geoinformation, 2016, 44, 95-103.	1.4	12
110	Fluid flow simulations for the safety injection of carbon dioxide in Gundih CCS site, Indonesia. , 2015, , .		0
111	Time-lapse seismic profiles derived from passive seismic interferometry in fluid-injection experiments. , 2015, , .		3
112	Impact of interfacial tension on residual CO ₂ clusters in porous sandstone. Water Resources Research, 2015, 51, 1710-1722.	1.7	38
113	Geological characteristic and fault stability of the Gundih CCS pilot project at central Java, Indonesia. , 2015, , .		3
114	Advanced surface-wave analysis for 3D ocean bottom cable data to detect localized heterogeneity in shallow geological formation of a CO2 storage site. International Journal of Greenhouse Gas Control, 2015, 39, 107-118.	2.3	18
115	QP structure of the accretionary wedge in the Kumano Basin, Nankai Trough, Japan, revealed by long-offset walk-away VSP. Earth, Planets and Space, 2015, 67, 7.	0.9	7
116	Identification of the static backstop and its influence on the evolution of the accretionary prism in the Nankai Trough. Earth and Planetary Science Letters, 2015, 431, 15-25.	1.8	49
117	Characteristics of the horizontal component of Rayleigh waves in multimode analysis of surface waves. Geophysics, 2015, 80, EN1-EN11.	1.4	22
118	Lattice Boltzmann Simulations of Supercritical CO ₂ –Water Drainage Displacement in Porous Media: CO ₂ Saturation and Displacement Mechanism. Environmental Science & Technology, 2015, 49, 537-543.	4.6	75
119	Hydrothermal Activity in the Okinawa Trough Back-Arc Basin: Geological Background and Hydrothermal Mineralization. , 2015, , 337-359.		43
120	Active Rifting Structures in Iheya Graben and Adjacent Area of the Mid-Okinawa Trough Observed Through Seismic Reflection Surveys. , 2015, , 361-368.		6
121	Characterization of near-surface heterogeneity by integrating surface-wave phase velocity and attenuation. , 2015, , .		2
122	Natural surface rebound of the Bangkok plain and aquifer characterization by persistent scatterer interferometry. Geochemistry, Geophysics, Geosystems, 2014, 15, 965-974.	1.0	24
123	Potential Evaluation of CO2 Reservoir Using the Measured Petrophysical Parameter of Rock Samples in the Gundih CCS Project, Indonesia. Energy Procedia, 2014, 63, 4965-4970.	1.8	6
124	Reservoir Characterization for site Selection in the Gundih CCS Project, Indonesia. Energy Procedia, 2014, 63, 6335-6343.	1.8	19
125	Gas hydrate saturation at <scp>S</scp> ite <scp>C</scp> 0002, <scp>IODP E</scp> xpeditions 314 and 315, in the <scp>K</scp> umano <scp>B</scp> asin, <scp>N</scp> ankai trough. Island Arc, 2014, 23, 142-156.	0.5	52
126	Changes in pore geometry and relative permeability caused by carbonate precipitation in porous media. Physical Review E, 2014, 90, 053306.	0.8	48

#	Article	IF	CITATIONS
127	Strike-slip motion of a mega-splay fault system in the Nankai oblique subduction zone. Earth, Planets and Space, 2014, 66, 120.	0.9	38
128	Misfit functionals in Laplaceâ€Fourier domain waveform inversion, with application to wideâ€angle ocean bottom seismograph data. Geophysical Prospecting, 2014, 62, 1054-1074.	1.0	20
129	Pore pressure distribution of a mega-splay fault system in the Nankai Trough subduction zone: Insight into up-dip extent of the seismogenic zone. Earth and Planetary Science Letters, 2014, 396, 165-178.	1.8	100
130	Elucidating the Role of Interfacial Tension for Hydrological Properties of Two-Phase Flow in Natural Sandstone by an Improved Lattice Boltzmann Method. Transport in Porous Media, 2014, 104, 205-229.	1.2	51
131	Lithology-controlled subsidence and seasonal aquifer response in the Bandung basin, Indonesia, observed by synthetic aperture radar interferometry. International Journal of Applied Earth Observation and Geoinformation, 2014, 32, 199-207.	1.4	9
132	Azimuthal anisotropy of Rayleigh waves in the crust in southern Tohoku area, Japan. Journal of Geophysical Research: Solid Earth, 2014, 119, 8964-8975.	1.4	4
133	Preliminary Feasibility Study for On-Site Hydrogen Station with Distributed CO2 Capture and Storage System. Energy Procedia, 2014, 63, 4575-4584.	1.8	6
134	Interfacial Tension Effect on Cluster Size Distributions for Residual Trapping of CO2 in Sandstones. Energy Procedia, 2014, 63, 5483-5489.	1.8	2
135	The study of heterogeneous twoâ€phase flow around smallâ€scale heterogeneity in porous sandstone by measured elastic wave velocities and lattice Boltzmann method simulation. Journal of Geophysical Research: Solid Earth, 2014, 119, 7564-7577.	1.4	12
136	Seismic-Derived Quality Factor for Lithology Classification around the Median Tectonic Line. Zairyo/Journal of the Society of Materials Science, Japan, 2014, 63, 250-257.	0.1	2
137	Difference in acoustic properties at seismogenic fault along a subduction interface: Application to estimation of effective pressure and fluid pressure ratio. Tectonophysics, 2013, 600, 134-141.	0.9	8
138	Extension of continental crust by anelastic deformation during the 2011 Tohoku-oki earthquake: The role of extensional faulting in the generation of a great tsunami. Earth and Planetary Science Letters, 2013, 364, 44-58.	1.8	76
139	Effect of Reservoir Heterogeneity of Haizume Formation, Nagaoka Pilot Site, Based on High-resolution Sedimentological Analysis. Energy Procedia, 2013, 37, 3546-3553.	1.8	11
140	Widely distributed thrust and strike-slip faults within subducting oceanic crust in the Nankai Trough off the Kii Peninsula, Japan. Tectonophysics, 2013, 600, 52-62.	0.9	25
141	Episodic slow slip events in the Japan subduction zone before the 2011 Tohoku-Oki earthquake. Tectonophysics, 2013, 600, 14-26.	0.9	303
142	Singular-value decomposition analysis of source illumination in seismic interferometry by multidimensional deconvolution. Geophysics, 2013, 78, Q25-Q34.	1.4	18
143	Detection of Localized Surface Uplift by Differential SAR Interferometry at the Hangingstone Oil Sand Field, Alberta, Canada. IEEE Journal of Selected Topics in Applied Earth Observations and Remote Sensing, 2013, 6, 2344-2354.	2.3	11
144	On acoustic waveform tomography of wide-angle OBS datastrategies for pre-conditioning and inversion. Geophysical Journal International, 2013, 194, 1250-1280.	1.0	64

#	Article	IF	CITATIONS
145	Recent surface displacement in bangkok, Thailand inferred from persistent scatterer SAR interferometry. , 2013, , .		1
146	Monitoring and characterization of land subsidence in the Bandung Basin, West Java, Indonesia, using SAR interferometry. , 2013, , .		1
147	Multimode inversion of Rayleigh waves using vertical and horizontal component data. , 2013, , .		0
148	Characteristics of a tsunamigenic megasplay fault in the Nankai Trough. Geophysical Research Letters, 2013, 40, 4594-4598.	1.5	14
149	New packer experiments and borehole logs in upper oceanic crust: Evidence for ridgeâ€parallel consistency in crustal hydrogeological properties. Geochemistry, Geophysics, Geosystems, 2013, 14, 2900-2915.	1.0	14
150	Window-controlled CMP crosscorrelation analysis for surface waves in laterally heterogeneous media. Geophysics, 2013, 78, EN95-EN105.	1.4	48
151	Improved correlation analysis to detect liquefied area using multi-temporal SAR images —Application to the 2011 Tohoku Earthquake and the 2011 Christchurch Earthquake—. BUTSURI-TANSA(Geophysical Exploration), 2013, 66, 25-35.	0.0	Ο
152	Long offset walkaway and circle VSP in Nankai trough seismogenic zone. , 2013, , .		0
153	Elastic Properties of Lunar Regolith from Vertical Seismic Profiling. , 2012, , .		3
154	Crosscorrelation of Earthquake Data Using Stationary Phase Evaluation: Insight into Reflection Structures of Oceanic Crust Surface in the Nankai Trough. International Journal of Geophysics, 2012, 2012, 1-8.	0.4	9
155	Detection and mapping of soil liquefaction in the 2011 Tohoku earthquake using SAR interferometry. Earth, Planets and Space, 2012, 64, 1267-1276.	0.9	28
156	Surface-wave analysis for identifying unfrozen zones in subglacial sediments. Geophysics, 2012, 77, EN17-EN27.	1.4	40
157	Waveform tomography imaging of a megasplay fault system in the seismogenic Nankai subduction zone. Earth and Planetary Science Letters, 2012, 317-318, 343-353.	1.8	115
158	Runaway slip to the trench due to rupture of highly pressurized megathrust beneath the middle trench slope: The tsunamigenesis of the 2011 Tohoku earthquake off the east coast of northern Japan. Earth and Planetary Science Letters, 2012, 339-340, 32-45.	1.8	81
159	Monitoring seismic velocity change caused by the 2011 Tohokuâ€oki earthquake using ambient noise records. Geophysical Research Letters, 2012, 39, .	1.5	85
160	Geomechanical modeling for InSAR-derived surface deformation at steam-injection oil sand fields. Journal of Petroleum Science and Engineering, 2012, 96-97, 152-161.	2.1	19
161	Global optimisation by simulated annealing for common reflection surface stacking and its application to low-fold marine data in southwest Japan. Exploration Geophysics, 2012, 43, 59-69.	0.5	15

Borehole Geotechnical Testing Tool for Lunar Exploration. , 2012, , .

#	Article	IF	CITATIONS
163	Multimode inversion with amplitude response of surface waves in the spatial autocorrelation method. Geophysical Journal International, 2012, 190, 541-552.	1.0	53
164	Hydrothermal fluid flow system around the Iheya North Knoll in the mid-Okinawa trough based on seismic reflection data. Journal of Volcanology and Geothermal Research, 2012, 213-214, 41-50.	0.8	71
165	Seismic interferometry using multidimensional deconvolution and crosscorrelation for crosswell seismic reflection data without borehole sources. Geophysics, 2011, 76, SA19-SA34.	1.4	47
166	In situ stress state from walkaround VSP anisotropy in the Kumano basin southeast of the Kii Peninsula, Japan. Geochemistry, Geophysics, Geosystems, 2011, 12, n/a-n/a.	1.0	20
167	Frontal wedge deformation near the source region of the 2011 Tohoku-Oki earthquake. Geophysical Research Letters, 2011, 38, n/a-n/a.	1.5	232
168	<i>V</i> _P / <i>V</i> _S ratio and shear-wave splitting in the Nankai Trough seismogenic zone: Insights into effective stress, pore pressure, and sediment consolidation. Geophysics, 2011, 76, WA71-WA82.	1.4	79
169	Acceleration of computation speed for elastic wave simulation using a Graphic Processing Unit. Exploration Geophysics, 2011, 42, 98-104.	0.5	20
170	Shearâ \in wave imaging from traffic noise using seismic interferometry by crossâ \in coherence. , 2011, , .		4
171	Interpretation of the effect of source-receiver configuration for Seismic interferometry by Multidimensional deconvolution using singular-value decomposition. , 2011, , .		Ο
172	The Relationship between Permeability and Elastic Modulus of Ellipsoidally-Cracked Rock Model. , 2011, , ,		0
173	Singularâ€value decomposition analysis for seismic interferometry by multidimensional deconvolution. , 2011, , .		1
174	Shear wave imaging from traffic noise using seismic interferometry by cross-coherence. Geophysics, 2011, 76, SA97-SA106.	1.4	218
175	Potential tsunamigenic faults of the 2011 off the Pacific coast of Tohoku Earthquake. Earth, Planets and Space, 2011, 63, 831-834.	0.9	67
176	Surface wave analysis for studying elastic properties of glacier bed sediments. , 2011, , .		0
177	The interpretation for structure of three-dimensional Splay Fault in Nankai trough. , 2011, , .		Ο
178	Potential Tsunamigenic Faults of the 2011 Tohoku Earthquake in the Frontal Wedge. , 2011, , .		0
179	Evaluation of Vibration Characteristics at Improved Soft Ground by Surface Wave Method. , 2011, , .		Ο
180	Soil liquefaction at water front area associated with 2011 Tohoku earthquake; Insight from DInSAR analysis. , 2011, , .		0

#	Article	IF	CITATIONS
181	The proposed inversion technique of remote sensing data for reservoir monitoring , 2011, , .		Ο
182	Multi-mode analysis of Spatial Auto Correlation (SPAC) method considering different correlation distance. BUTSURI-TANSA(Geophysical Exploration), 2011, 64, 127-138.	0.0	2
183	Waveform Tomography Imaging of Deep Crustal Faults - Application to Nankai Subduction Zone. , 2011, ,		Ο
184	Mineral classification from quantitative Xâ€ray maps using neural network: Application to volcanic rocks. Island Arc, 2010, 19, 105-119.	0.5	13
185	Higher modes of surface waves in microtremor analysis. , 2010, , .		1
186	Hydrothermal plumes imaged by highâ€resolution sideâ€scan sonar on a cruising AUV, <i>Urashima</i> . Geochemistry, Geophysics, Geosystems, 2010, 11, .	1.0	41
187	Vp/Vs and shearâ€wave splitting at the seismogenic plate subduction zone: Insight into effective―stress and pore pressure distribution. , 2010, , .		0
188	Estimation of detailed temperature distribution of sea water using seismic oceanography. BUTSURI-TANSA(Geophysical Exploration), 2009, 62, 509-520.	0.0	3
189	Earthquake fault of the 26 May 2006 Yogyakarta earthquake observed by SAR interferometry. Earth, Planets and Space, 2009, 61, e29-e32.	0.9	47
190	Intraoceanic thrusts in the Nankai Trough off the Kii Peninsula: Implications for intraplate earthquakes. Geophysical Research Letters, 2009, 36, .	1.5	18
191	Application of seismic interferometry by multidimensional deconvolution to crosswell seismic reflection using singularâ€value decomposition. , 2009, , .		5
192	Shear-wave velocity and splitting within the Nankai accretionary prism off the Kii Peninsula: Insight into effective-stress and pore-pressure distribution. , 2009, , .		1
193	Effective stress and pore pressure in the Nankai accretionary prism off the Muroto Peninsula, southwestern Japan. Journal of Geophysical Research, 2008, 113, .	3.3	88
194	Velocity-porosity relationships in oceanic basalt from eastern flank of the Juan de Fuca Ridge: The effect of crack closure on seismic velocity. Exploration Geophysics, 2008, 39, 41-51.	0.5	39
195	Large-scale convolute lamination and flame structures in the Plio-Pleistocene Hata Formation, Chikura Group, central Japan. Journal of the Geological Society of Japan, 2007, 113, XVII-XVIII.	0.2	Ο
196	Dependence of Toroidal Current on Bumpy Field Component in Heliotron J. Fusion Science and Technology, 2007, 51, 122-128.	0.6	3
197	Oceanic crust and Moho of the Pacific Plate in the eastern Ogasawara Plateau region. Island Arc, 2007, 16, 361-373.	0.5	18
198	Modern and ancient seismogenic out-of-sequence thrusts in the Nankai accretionary prism: Comparison of laboratory-derived physical properties and seismic reflection data. Geophysical Research Letters, 2006, 33, n/a-n/a.	1.5	27

#	Article	IF	CITATIONS
199	Configuration Control for the Confinement Improvement in Heliotron J. Fusion Science and Technology, 2006, 50, 352-360.	0.6	11
200	Simultaneous seismic reflection and physical oceanographic observations of oceanic fine structure in the Kuroshio extension front. Geophysical Research Letters, 2006, 33, .	1.5	61
201	Pore pressure prediction near the plate boundary fault in the Nankai Trough, southwest Japan: Insight from seismic interval velocity and well data. , 2006, , .		0
202	Seismic and Physical Oceanographic Joint Observation for Oceanic Finestructure in the Kuroshio Extension Front , 2006, , .		0
203	Initiation of plate boundary slip in the Nankai Trough off the Muroto peninsula, southwest Japan. Geophysical Research Letters, 2005, 32, n/a-n/a.	1.5	23
204	Two-dimensional mapping of fine structures in the Kuroshio Current using seismic reflection data. Geophysical Research Letters, 2005, 32, n/a-n/a.	1.5	53
205	Effects of vibrational excitation of target N2 molecule in charge–transfer reaction of He+ with N2 at thermal energy. Journal of Chemical Physics, 2001, 115, 6811-6814.	1.2	3
206	D. ãf¬ãf¼ã,¶ãf¼ãf—ãfã,»ã,•ãf³ã,°. The Review of Laser Engineering, 2000, 28, 89-97,103.	0.0	0
207	Investigation of intramolecular hydrogen bonds in ortho-hydroxytropolone. Journal of Chemical Physics, 1999, 110, 966-971.	1.2	8
208	Fluorescence Excitation and Hole-Burning Spectra of Jet-Cooled Tropoloneâ^'M (M = N2, CO) van der Waals Complexes:  Structures and Proton Tunneling in the S1 State. Journal of Physical Chemistry A, 1998, 102, 3880-3888.	1.1	16
209	Tunneling splittings in the S1 electronic states of symmetrically substituted 3,7â€dichlorotropolone, 3,5,7â€ŧrichlorotropolone, and 3,7â€dibromotropolone. Journal of Chemical Physics, 1994, 101, 3464-3471.	1.2	26
210	Electronic spectra of jetâ€cooled 3―and 4â€chlorotropolones in the S1–S0 region. Inhibition of proton tunneling by asymmetric substitution. Journal of Chemical Physics, 1993, 98, 6571-6573.	1.2	18
211	Electronic spectra of jetâ€cooled 5â€bromotropolone and 5â€chlorotropolone. Influence of symmetrical substitution on proton tunneling in the S1 state. Journal of Chemical Physics, 1992, 97, 6032-6039.	1.2	40
212	Electronic spectra of jetâ€cooled 3â€chlorotropolone. Proton tunneling in the S1 state. Journal of Chemical Physics, 1991, 95, 4802-4808.	1.2	16
213	Thermal fluid migration in the Kumano forearc basin, Nankai Trough, estimated via vitrinite reflectance measurement. , 0, , .		1
214	Structural and seismic stratigraphic framework of the NanTroSEIZE Stage 1 transect. Proceedings of the Integrated Ocean Drilling Program Integrated Ocean Drilling Program, 0, , .	1.0	139
215	IODP Expedition 327 and <i>Atlantis</i> Expedition AT 18-07: Observatories and Experiments on the Eastern Flank of the Juan de Fuca Ridge. Scientific Drilling, 0, 13, 4-11.	1.0	6
216	Site C0025. Proceedings of the International Ocean Discovery Program, 0, , .	0.0	2